Journal of Applied Geophysics 153 (2018) 100–112

Contents lists available at ScienceDirect

Journal of Applied Geophysics

journal homepage: www.elsevier.com/locate/jappgeo

Improvement of 2D ERT measurements conducted along a small earth-filled dyke using 3D topographic data and 3D computation of geometric factors

Grégory Bièvre [a,*], Laurent Oxarango [b], Thomas Günther [c], David Goutaland [d], Michael Massardi [e]

[a] Univ. Grenoble Alpes, Univ. Savoie Mont Blanc, CNRS, IRD, IFSTTAR, ISTerre, F-38000 Grenoble, France
[b] Univ. Grenoble Alpes, CNRS, IRD, Grenoble-INP, IGE, F-38000 Grenoble, France
[c] Leibniz Institute for Applied Geophysics, 30655 Hanover, Germany
[d] CEREMA, Direction Territoriale Centre-Est, Laboratoire de Clermont-Ferrand, F-63017 Clermont-Ferrand, France
[e] CEREMA, Direction Territoriale Centre-Est, Laboratoire d'Autun, F-71405 Autun, France

ARTICLE INFO

Article history:
Received 28 June 2017
Received in revised form 22 February 2018
Accepted 12 April 2018
Available online 14 April 2018

Keywords:
Earth-filled dyke
ERT
Geometric factor
Numerical simulation
Monitoring

ABSTRACT

In the framework of earth-filled dykes characterization and monitoring, Electrical Resistivity Tomography (ERT) turns out to be a commonly used method. 2D sections are generally acquired along the dyke crest thus putting forward the question of 3D artefacts in the inversion process. This paper proposes a methodology based on 3D direct numerical simulations of the ERT acquisition using a realistic topography of the study site. It allows computing ad hoc geometrical factors which can be used for the inversion of experimental ERT data. The method is first evaluated on a set of synthetic dyke configurations. Then, it is applied to experimental static and time-lapse ERT data set acquired before and after repair works carried out on a leaking zone of an earth-filled canal dyke in the centre of France. The computed geometric factors are lower than the analytic geometric factors in a range between −8% and − 18% for measurements conducted on the crest of the dyke. They exhibit a maximum under-estimation for intermediate electrode spacings in the Wenner and Schlumberger configurations. In the same way, for measurements conducted on the mid-slope of the dyke, the computed geometric factors are higher for short electrode spacings (+18%) and lower for lower for large electrode spacings (−8%). The 2D inversion of the synthetic data with these computed geometric factors provides a significant improvement of the agreement with the original resistivity. Two experimental profiles conducted on the same portion of the dyke but at different elevations also reveal a better agreement using this methodology. The comparison with apparent resistivity from EM31 profiling along the stretch of the dyke also supports this evidence. In the same way, some spurious effects which affected the time-lapse data were removed and improved the global readability of the time-lapse resistivity sections. The benefit on the structural interpretation of ERT images remains moderate but allows a better delineation of the repair work location. Therefore, and even if the 2D assumption cannot be considered valid in such a context, the proposed methodology could be applied easily to any dyke or strongly 3D-shaped structure using a realistic topographic model. It appears suitable for practical application.

1. Introduction

Earth-filled embankments are worldwide-spread structures. Some of them might be older than several centuries and, consequently, their geotechnical condition might be very poorly known. As such, there is a need for rapid, cost-effective and noninvasive tools, making geophysical methods adequate for such investigations. In the past decades, Electrical Resistivity Tomography (ERT) has become one of the most popular geophysical techniques to investigate such structures. It allows imaging in high-resolution the depth to the bedrock and the lateral variation of the interface between the dyke and its substratum (Cardarelli et al., 2010; Minsley et al., 2011; Cardarelli et al., 2014; Bièvre et al., 2017). This technique can also provide information about the internal structure of the dykes (Weller et al., 2006; Cho & Yeom, 2007; Niederleithinger et al., 2012). Measurements can also be repeated to provide the evolution of resistivity with time. This time-lapse approach is used to derive the evolution of a physical parameter to which resistivity is sensitive (temperature, clay content, moisture, etc.). This approach was used by several authors to locate seepage paths within earth dykes (Sjödahl et al., 2008; Sjödahl et al., 2009; Weller et al., 2014).

* Corresponding author.
E-mail address: gregory.bievre@univ-grenoble-alpes.fr. (G. Bièvre).

https://doi.org/10.1016/j.jappgeo.2018.04.012
0926-9851/

However, for practical considerations such as cost-effectiveness and available space, electrodes are generally spread along the dyke crest. This configuration might appear very well suited to try to detect weak zones, where seepage paths could exist at depth and which are generally perpendicular to the dyke stretch and, consequently, to the electrode spread. Classically, dyke crests are considered as flat structures and analytical geometric factors, defined for infinite flat half-spaces, are used to compute apparent resistivity. Thus, data are processed using 2D inversion algorithms which do not take into account the 3D geometric effects caused by the topography, and the 3D geophysical effects caused by the subsurface resistivity distribution. The effect of topography was reported and evaluated in 2D since more than thirty-five years in the pioneering works of Fox et al. (1980). However, such effects remain little studied specifically in the context of dykes monitoring. Hennig et al. (2005) studied the effect of topography on resistivity measurements for several protocols and for profiles acquired perpendicular to the stretch of a dyke. Using Finite Element Modelling, they were able to determine a factor to correct resistivity measurements from the effect of surface geometry. A very similar approach will be used in this work. Sjödahl et al. (2006) numerically studied a 220 m wide and 60 m high dam made of a till core, a surrounding filter zone, and a rock cap. Using a 2.5 D approach (a 2D model with a constant geometry in the third dimension), they showed that the 3D geometric setting affected the data. When compared with a 1D model, the computed resistivity increased from around 20% to almost 40% as a function of electrode spacing. They also showed that the variation of the water level in the reservoir had an effect on the computed resistivity. Their work finally showed that it is possible to assess these effects using numerical computation. Similarly, Cho et al. (2014) numerically studied topographic effects on a 86 m wide and 20 m high earth dyke. They evidenced resistivity variations of up to 30% caused by water level fluctuations. They chose to build a combined reference model to invert experimental time-lapse data. This strategy allowed to detect a damaged zone for low water level change but failed to image it for large water level change. Recently, Fargier et al. (2014) studied numerically and experimentally such geometric effects on a smaller structure, namely an earth-filled dyke with a height of 6 m and a width of 28 m. They confirmed the existence of 3D geometric effects and proposed to correct them by using the computation of topographic (i.e. surface geometry) effects but also by using a priori information regarding the 3D resistivity distribution of the sub-surface.

Bièvre et al. (2017) recently reported an integrated geophysical (seismic and resistivity) and geotechnical study of a small earth-filled canal dyke (10 m wide at the base and a maximum height of 10 m) located in the centre of France. This study allowed to define precisely the geotechnical configuration of the dyke and also to locate a seepage path at a depth of around 3.4 m below the dyke crest using ambient vibrations. However, static ERT failed to locate this seepage and even exhibits a seemingly incoherent discrepancy between parallel profiles conducted at different elevations.

The aim of this study is first to numerically evaluate the origin of such a poor performance of ERT in the context of dykes. The direct current electrical diffusion problem is solved using 3D finite element synthetic models simulating the studied dyke. Increasing levels of complexity are considered to evaluate the effect of topography and of 3D/4D resistivity distributions (e.g. a change in the water level in the canal). Such an approach allows computing custom geometric factors and to assess their benefit on the 2D inversion. The second objective is to process experimental static and time-lapse data using these computed geometric factors before a classical 2D inversion. The variation of the water level in the canal induced time-varying topography and resistivity variations during the study. These corrected results are then compared with the results of a classic 2D time-lapse approach in order to put forward the ability of this approach to retrieve more realistic resistivity which can help imaging and monitoring earth dykes more accurately.

2. Materials and methods

2.1. Study site

The study site is located in the centre of France. The dyke was built during the first half of the XIXth century and is made of a heterogeneous mixture of silts, sands, and gravels which overly Jurassic marly limestones (Fig. 1a and b). The dyke's crest is 4 m large with a maximum height of 10 m. A 5 m-long breach occurred in 2007, which supposedly originated from internal erosion phenomena. The study area is located 1.5 km North of the breach, in an area where two apparently cylinder-shaped leakage zones (LZ) were visually identified (Fig. 1a). LZ1 and LZ2 showed water flow rates of around 250 l/min and of around a few tens of l/min, respectively. A 127 m-long profile was specifically selected on the crest of the dyke in order to test different surface geophysical methods (refraction seismics, P-wave and S-wave tomography, surface waves inversion, Electrical Resistivity Tomography). It corresponds to electrical profile EP1 in Fig. 1 and, in the following, all distances are expressed with reference to this profile. This profile was selected because it covered two leakage zones (a major one at 35–45 m and a smaller one at 90–100 m along the profile and at depths of 3.4 m and 1.5 m below the top of the dyke, respectively; Fig. 1). Results were reported by Bièvre et al. (2017) and showed that these classical methods are able to retrieve the geometry of the dyke over the bedrock but failed to locate the two leakage zones. On the contrary, passive seismic monitoring allowed to localize LZ1 below the dyke crest, at a distance of 37 m $\pm$ 0.4 m along EP1 and a depth of 3 m $\pm$ 0.4 m. This depth corresponds to the interface between the dyke itself and the underlying bedrock. Using the same approach, LZ2 was not detected. It was then suggested that LZ1 was subject to turbulent water flows which allowed to generate energetic enough seismic signals.

2.2. 2D experimental ERT measurements

The 128 electrodes used for profile EP1 were left into the ground to periodically monitor the evolution of resistivity. A second ERT profile labelled EP2 (location in Fig. 1) was acquired on November the 10th 2010. It is located along the road, around 1.8 m below the top of the dyke. It consisted of 64 electrodes with a constant electrode spacing of 1 m. Four further roll-along allowed to gather a 127 m-long profile, with the same characteristics as EP1. The canal was emptied to repair the leakage zones (by injecting clays) and was then refilled. These work operations lasted four weeks between November the 08th and December the 12th, 2010.

Resistivity measurements were conducted with a single-channel ABEM Terrameter LS using 64 electrodes at a time. Four further roll-along steps with a shift of 16 electrodes were needed to complete the measurements. Given the technical limitations (single-channel resistivimeter), the Wenner-Schlumberger configuration was chosen since it provides both good vertical resolution and good signal-to-noise ratio (SNR). The vertical resolution was favoured to better detect the interface between the dyke and the bedrock. The good SNR was also chosen in order to detect even slight changes between time steps. To achieve a sufficiently satisfying lateral resolution, the number of measurements was set to a relatively high number (see further). The spacing between potential electrodes (a spacing) was set between 1 m and 21 m. For the Schlumberger configuration, the n factor was set between 2 and 7. Only the measurements in common between the sequences were kept for time-lapse processing. A total number of 3558 measurements was obtained, 983 of which were in a Wenner configuration (27% of the measurements).

Experimental injection parameters were set to 100–400 mA and 100–200 V for the required current and voltage between dipole AB, respectively. These parameters allowed to measure voltages between 0.05 V and 6 V for dipole MN. Most measurements indicated contact

resistances between 100 Ω and 200 Ω, except two electrodes between 500 Ω and 1000 Ω, indicating a good electrical coupling between the electrodes and the ground.

Finally, ERT measurements were conducted with varying hydrostatic water levels into the canal (Fig. 2). Measurements 0 and 4 were acquired with a water table located 0.7 m below the dyke crest (corresponding to a water height of 3 m into the canal). Measurement 1 was acquired with a water table located 1.85 m below the dyke crest (water level of 1.85 m into the canal) and measurements 2 and 3 were acquired with no water into the canal (hydrostatic level deeper than 3.7 m below the dyke crest).

It is well-known that resistivity is influenced by temperature (among many others: Waxman & Thomas, 1974; Hayley et al., 2007). As such, it has to be taken into account, especially for time-lapse measurements. Several exponential or linear relationships have been proposed to account for these variations but it can be evaluated as a 2% increase in resistivity for a decrease of 1 °C (Samouëlian et al., 2005; Hayley et al., 2007). Several methods have also been used to correct resistivity data from temperature variations: before (Hayley et al., 2010) or after inversion (e.g. Hayley et al., 2007; Bièvre et al., 2012). A drilling has been especially conducted for borehole temperature measurements on the study site, near the centre of the ERT profile. Unfortunately, technical issues did not allow to record sufficient measurements to get temperature logs for each time step and only the temperature log of November 12, 2010, is available. It has been then chosen to reduce the set of ERT time sections presented here to a period of 1 month before, during and after repair works. With this short time range, it is possible to consider resistivity data as weakly influenced by temperature changes at depths of some few metres. Resistivity sections were then standardized to a temperature of 10 °C, using the temperature log aforementioned to correct all resistivity measurements. The temperature correction strategy used in this work is provided as a supplementary material to this article.

Inversion of synthetic and experimental data was conducted using the Boundless Electrical Resistivity Tomography (BERT) algorithm developed by Günther et al. (2006) based on finite element computations on irregular triangles (Rücker et al., 2006). The regularization strength (Lambda) was manually tuned to get a Chi^2 value close to 1, indicating that the data were fitted within a default error of 3%. Synthetic data were inverted using a homogeneous starting model with a resistivity of 400 Ω.m. For the time-lapse approach, successive experimental apparent resistivity sections were inverted using the difference inversion method proposed by LaBrecque & Yang (2001). Time-lapse results are presented as resistivity ratio with respect to the reference acquisition (measurement 1 in Fig. 2).

2.3. Electromagnetic profiling

The apparent resistivity of the dyke was measured with another tool to compare the efficiency of the geometric corrections to retrieve more realistic resistivity. An electromagnetic (EM) profile was acquired along EP1 using an EM31 conductivity meter (Geonics Ltd., Mississauga, Canada). The fundamentals of the technique are provided in reference books (e.g. Telford et al., 1990) and specifics about the device can be found in McNeill (1980). The apparent resistivity was measured at each electrode location along the 127 m-long profile. At each station, 100 measurements were taken (at a period of 0.5 s) and the mean resistivity was calculated. The mean relative standard deviation of the measurements at each station is 1%, indicating that the site exhibits few EM noise. Profiles were acquired with vertical coplanar loops (estimated maximum investigation depth between around 2 m and 3 m) to investigate the dyke only. It must be pointed out that the apparent conductivity is calculated assuming a homogeneous and flat half-space model. Given the geometry of the dyke (Fig. 1b), the measured resistivity cannot be considered as the true resistivity. From our experience, however, and from the geometry of the acquisition (coils aligned along the dyke stretch with a separation of 3.66 m, measurements conducted along a 4 m-width dyke on the crest and with a slope of 33%), it is hypothesized that this geometric effect can be considered as negligible. Measurements were acquired November 03, 2010. Results were compared with the mean resistivity of the first 2 m below ground extracted from ERT profile EP1 acquired November 09, 2010 (measurement 1 in Fig. 2).

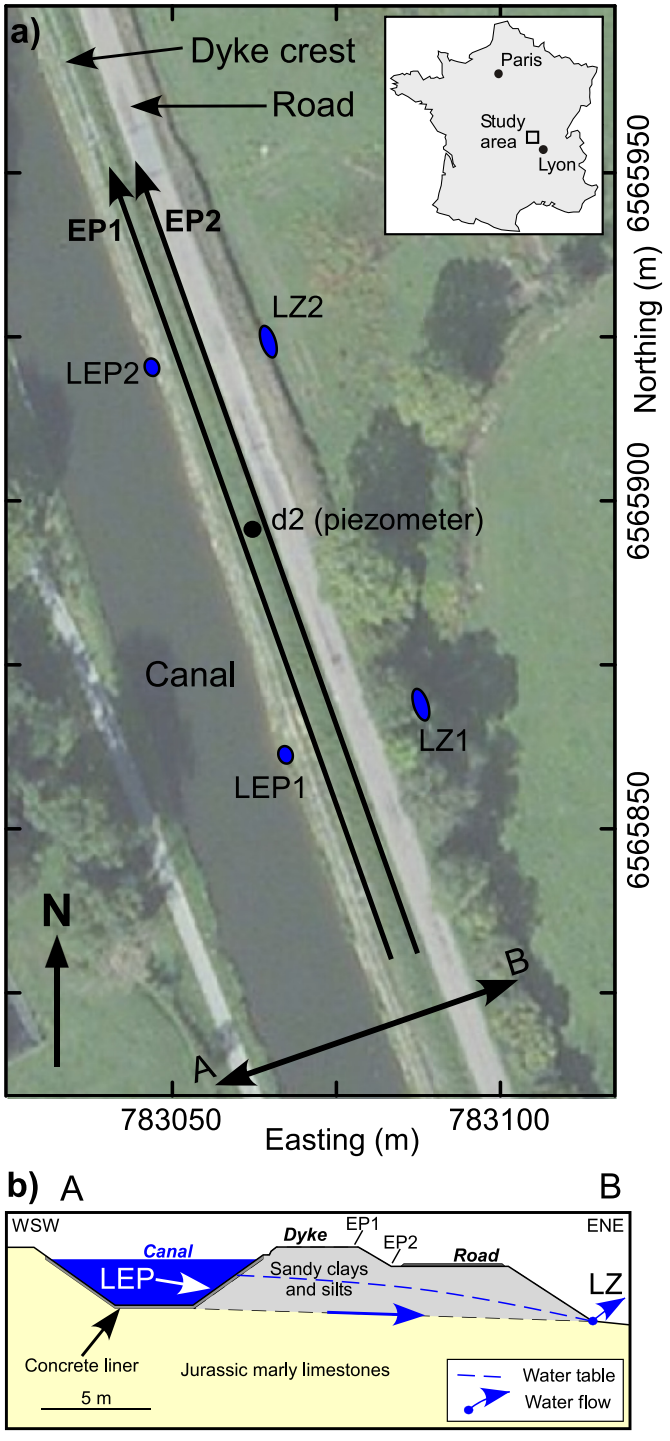

Fig. 1. Location of the study site. a) Location of the geophysical measurements EP1 and EP2. The location of the two main leakage zones is indicated (LEP: Leakage Entry Path; LZ: Leakage Zone). Coordinates are expressed in the Lambert93 French system. b) Conceptual cross-section AB of the dyke.

2.4. Numerical modelling of ERT measurements

In order to investigate the influence of 3D effects on the experimental ERT results, ERT measurements were simulated numerically on a simplified but realistic 3D configuration of the study site. This theoretical study is designed to evaluate the distortion of the electric field due to the 3D topography of the site, the effect of the water filling the canal and the heterogeneous nature of the embankment and substratum materials.

2.4.1. Mathematical model and simulation strategy

The numerical computations were conducted with the Matlab F3DM package (Clément & Moreau, 2016) coupling Matlab 2014 and Comsol Multiphysics 5.2 software. The finite element (FE) solver Comsol Multiphysics is used to solve the stationary electric conduction problem reading as:

$$\nabla.J = -\nabla.(\sigma\nabla V) = q_i, \tag{1}$$

where J is the current density vector (A/m^2), σ is the electrical conductivity (S/m), V is the electric potential (V), and q_i is a volumetric current source (A/m^3). This current source is kept at 0 except at the FE nodes used to model the current injection electrodes. Neumann boundary conditions (no flux) are imposed on all the surface boundaries considering that the atmospheric boundary is infinitely resistant and that the lateral and bottom boundaries are located at an infinite distance from the current source. It reads as:

$$J.n = 0 \tag{2}$$

where n is a normal unit vector of the boundary. Each quadrupole acquisition is then simulated by imposing punctually a positive current Q_i (A) at the node of electrode A and a negative current -Q_i (A) at the node of electrode B. The voltage for dipole MN is calculated on the computed electric field at the node corresponding to the electrode location as ($V_{MN} = V_M$-V_N). The F3DM package performs a sequential automated computation of the ERT acquisition sequence. This Matlab script first defines the location of electrodes AB and MN in the Comsol script file. Then, it launches the FE computation of the problem (Eqs. (1) and (2)). Finally, it stores the MN voltage results. At the end of the sequence, the output file constitutes a synthetic ERT data set that could be analyzed using the same inversion methodology as a classical experimental ERT data set.

2.4.2. Domain configurations and meshing

The spatial domain for computation is a large parallelepiped of dimension Xm × Ym × Zm (Fig. 3a). Its dimensions have been chosen after a domain size sensitivity set of computations in order to obtain a neglectable effect of boundaries on the electric potential distribution. The dyke and canal geometry has been designed in agreement with the average topography measured on the study site (Figs. 3a, b and 4). The tetrahedral mesh (Fig. 3) is generated by Comsol Multiphysics. A strong refinement is applied close to each electrode and more generally on the dyke crest along the electrode line (see Fig. 3c for an example with profile EP1). On the other hand, the mesh is very loose away from the dyke for a total number of 151,138 tetrahedrons.

Four configurations have been tested in order to evaluate the effect of the 3D topography of the study site, the effect of the water filling the canal and the heterogeneous nature of the embankment and bedrock materials (Fig. 4). In the homogeneous configuration (ConfA), the resistivity is uniformly set at 50 Ω.m. In the heterogeneous cases (ConfB, ConfC and ConfD), the dyke resistivity has been set to 50 Ω.m based on shallow EM31 measurements, the water resistivity to 20 Ω.m based on a multi-parameter probe direct measurement and the substratum resistivity to 400 Ω.m based on the average value observed in experimental resistivity obtained from ERT (Bièvre et al., 2017).

2.4.3. Geometric factor computation

In most cases, the apparent resistivity is measured using a quadrupole consisting of two current-injecting electrodes (A and B) and two electrodes (M and N) to measure the resulting potential. The apparent resistivity is defined by:

$$\rho_a = K \cdot R = \frac{K \cdot V_{MN}}{I} \tag{4}$$

where ρ_a is the apparent resistivity in Ω.m, K is the geometric factor in m, R is the electrical resistance in Ω, V_{MN} is the electrical voltage between electrodes M and N (in V) and I is the electrical current (in A). For a quadrupole ABMN, the geometric factor K is analytically defined by:

$$K = 2\pi \cdot \left(\frac{1}{AM} - \frac{1}{BM} - \frac{1}{AN} + \frac{1}{BN}\right)^{-1} \tag{5}$$

and only depends on the electrode configuration. This definition is, however, valid for a flat surface with electrodes located at the surface only. Nevertheless, in the case of a complex surface morphology, it is

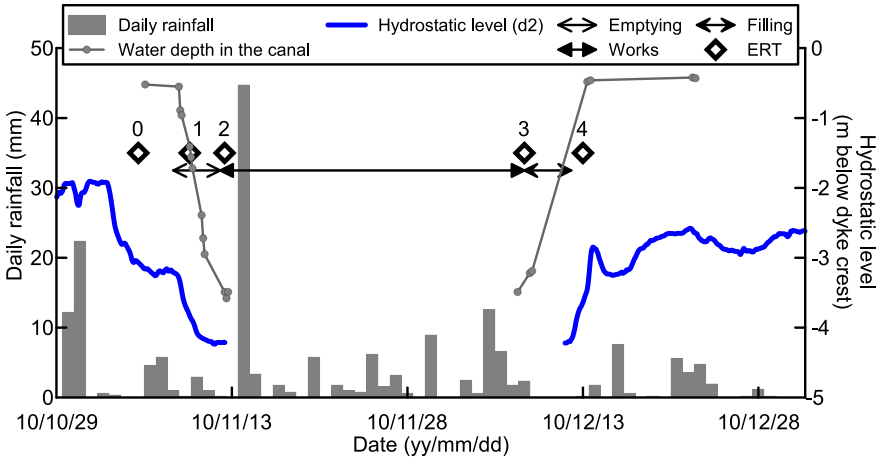

Fig. 2. Hydrostatic level within the canal and the dyke (d2), rainfall, dates of experiments, periods of water emptying, works and water filling.

Table 1
Hydrostatic level during ERT measurements.

Measurement	Date	Days since time-lapse Reference measurement 1	Hydrostatic level below dyke crest (m)	
			In the canal	In the dyke (d2)
0	2010/11/08	−1	0.7	3.25
1	2010/11/09	0	1.85	3.9
2	2010/11/12	3	> 3.7	> 4.2
3	2010/12/08	29	> 3.7	> 4.2
4	2010/12/13	34	0.7	3.3

possible to compute the geometric factor numerically. By rearranging Eq. (4), the geometric factor is numerically determined using:

$$K = \frac{\rho_a}{R} = \frac{\rho_a \cdot I}{V_{MN}} \tag{6}$$

Applying the same approach as Hennig et al. (2005), FEM computation provides the geometric factor of any object, using a model of homogeneous resistivity ρ and a known transmitted current. The resulting voltage V_{MN} is numerically computed and the geometric factor is then determined for each electrode configuration.

In the study case, the water level variation in the canal should lead to a variation of geometric factors and, hence, of apparent resistivity as shown by previous works (Sjödahl et al., 2006; Cho et al., 2014; Fargier et al., 2014). However, Eq. (6) is valid for a sub-surface with a constant resistivity only. Despite the obvious simplification, the empty canal configuration (ConfA in Fig. 4) has been modified to model the effect of an intermediate water level in the canal (located 1.85 m below the dyke crest) and for a water level in the canal located 0.3 m below the dyke crest, which corresponds to the level of service). The rationale behind this approach is to test the benefit of using customized geometric factors computed from the site topography only.

3. Results from synthetic modelling

3.1. Current density distributions

Fig. 5 presents the distribution of the electrical current density for two quadrupoles spreadings along the crest of a dyke of a maximum height of 6 m over a bedrock. The resistivity of the dyke and of the bedrock are 50 Ω.m and 400 Ω.m, respectively. Simulations were conducted for two water levels in the canal: 3.7 m and 0.3 m below the dyke crest, respectively. The resistivity of the water was set to 20 Ω.m after in situ conductivity measurements. Calculations were also conducted for two current electrode spacings (AB = 3 m and 63 m) corresponding to the minimum and maximum AB spacing for a conventional Wenner configuration with 64 electrodes with a constant spacing of 1 m. The cross-sections in Fig. 5 are located at the mid-point between electrodes A and B.

Results show that for a small AB spacing and no water into the canal, the electrical current mainly flows in the dyke below the electrodes (Fig. 5a). When water is present (Fig. 5b), the distribution of the current density does not fundamentally change but a part of the electrical current is flowing through the canal water. At depth, however, the bedrock is poorly investigated compared to the dyke. For a large AB spacing and no water in the canal, results show that most of the electrical current investigates a large width of the dyke (Fig. 5c). On the contrary, when water is present in the canal, most of the electrical current flows in the water and the sub-surface is poorly investigated (Fig. 5d). Furthermore, all these results show that the current is distributed not only below the electrodes, along the flat crest of the dyke, but along a section which exhibits laterally marked topographic variations.

Fig. 5e and f present the ratio of the electrical current density distribution with and without water in the canal for the two AB spacings 3 m (Fig. 5e) and 63 m (Fig. 5f). The white colour refers to a ratio arbitrarily chosen between 0.85 and 1.15. It reflects no major variation between the two models. The images reveal that for small AB spacing, the presence of water implies an important decrease of the current density (ratio as low as 0.2) in the dyke (and the bedrock) between 7 m and 14 m along the section. This is caused by the inlet of electrical current in the water in its upper right part (see Fig. 5b). The presence of water in the canal does not seem to have a major influence on the current distribution right below the electrodes. Fig. 5f shows that for a large AB spacing, the presence of water in the canal induces a general decrease (around 20%) of the current density below the dyke crest. The comparison of the two images (Fig. 5e and f) indicates that when water is present in the canal, the distribution of the current density is affected in a laterally varying way. This suggests that accompanying the topographical effect induced by the dyke geometry, the presence of water in the canal induces strong 3D effects on the current distribution when acquiring 2D measurements along the crest of the dyke.

3.2. Effects of topography and topographic corrections on apparent resistivity

First, the quality of the numerical model was evaluated. For this, a model consisting of a flat homogeneous half-space was built and the geometric factors were computed. The results were compared with those obtained from the analytic formula of Eq. (5). The mean relative difference is 0.003% with the strongest value (0.4%) occurring for the smallest electrode spacing (a = 1 m and $n = 1$). These results suggest that the numerical experiment provides results of satisfying quality.

The geometric factor was then calculated for varying geometric settings representing the different water levels in the canal during

Table 2
results of FEM calculations. RRMS: relative root mean square error. RSD: relative standard deviation.

Model	K	Iterations	Chi^2	RRMS (%)	Depth Range (m)	Model resistivity (ohm.m)					Result in Figure
						Min	Max	Mean	Median	RSD (%)	
ConfA	Analytical	4	1.09	5.34	X	55.2	64.6	60.1	60.2	2.26	7a
(Fig. 4a)	Corrected	2	1.02	3.68	X	41.8	52.4	49.9	50	2.8	7b
ConfB	Analytical	3	1	3.99	X	43	71	56.2	55.5	9.6	7c
(Fig. 4b)	Corrected	3	1	3.94	X	42	62	50.4	50.4	4.26	7d
ConfC	Analytical	4	1.08	4.73	0–6	51	278	63	58.7	20.9	7e
(Fig. 4c)					6–21	93	1505	595	497	65.6	
	Corrected	4	1.01	4.56	0–6	43	217	53.7	51.3	17	7f
					6–21	75	1674	595	467	74	
ConfD	Analytical	3	1.02	4	0–6	52.5	115	60	58	10.5	7 g
Fig. 4d)					6–21	73.7	1525	515	369	82	
	Corrected	4	1	4.2	0–6	44.5	150	52	50.8	13.5	7 h
					6–21	68	1126	415	324	71	

Table 3
Statistics on the inverted resistivity of profiles EP1 and EP2.

		Dyke			Bedrock		
		Mean	Standard deviation	Median	Mean	Standard deviation	Median
EP1 (Ω.m)	*Ka*	52	25	48	117	25	119
	Kc	46	27	44	105	26	108
EP2 (Ω.m)	*Ka*	36	32	34	80	39	69
	Kc	45	34	40	71	34	64
Relative difference Between EP1 And EP2 (%)	*Ka*	31	X	29	31.5	X	42
	Kc	2.2	X	9	32.5	X	41

experimental measurements. Since this work is dedicated to the topographic effect correction only, all the models were computed with a constant subsurface resistivity. Calculations were conducted with 3558 points per geometrical configuration (same quadrupoles as for experimental measurements). The discrepancy between equivalent ABMN configurations within each model was evaluated. The highest difference was found to be 0.27%. This value was obtained for the smallest electrode spacing in Wenner configuration (a = 1 m and $n = 1$). Once again, this value is indicative of the low level of numerical noise. Calculations were conducted for a ground with a constant resistivity for the three domain configurations. These three domains correspond to canal water depths below the dyke crest of 3.7 m, 1.85 m and 0.3 m. They correspond to experimental variations which occurred for different measurements of profile EP1. The same calculation was conducted for profile EP2, but only for a water level in the canal of 1.85 m below the dyke crest. This setting also corresponds to the experimental conditions during measurement of profile EP2 (November 10, 2010; see Fig. 2). Fig. 6 shows the relative difference ΔK between the computed geometric factor K_c and the analytic geometric factor K_a as a function of the spacing between current electrodes A and B (or pseudo-depth). ΔK is defined as:

$$\Delta K = \frac{(K_c - K_a)}{K_a} \cdot 100 \quad (7)$$

where ΔK is the percentage relative difference of the geometric factor (and, hence, of the measured apparent resistivity). For profile EP1, results first show that K_c is lower than K_a by 8% to 18% for both Wenner (Fig. 6a) and Schlumberger configurations (Fig. 6b). The evolution of ΔK exhibits a minimum for intermediate AB spacing between 4 m and 12 m. This minimum also depends on the electrode configuration and on the water level in the canal. The maximum underestimation varies between −16% and − 18%. This effect is significantly dependent on the water level in the canal. For both Wenner and Schlumberger configurations, the topographic effect increases as the water level in the canal decreases with differences of up to 6% for large electrode spacings. These results induce that resistivity is overestimated from 8% to 18% if no topographic correction is performed. They also suggest that this effect would lead to a noticeable and complex distortion of the resistivity distribution after inversion. Profile EP2 is located at an intermediate position on the flank of the dyke and the results exhibit a strong difference compared to profile EP1 (Fig. 6c for the Wenner configuration and Fig. 6d for the Schlumberger configuration). Contrarily to EP1, the evolution of ΔK is almost continuously decreasing, with overestimations of up to 18% for small AB spacings to underestimations down to −8% for large AB spacings. To summarize, this analysis of geometric factors indicates that geometrical effects could lead to distortions when performing time-lapse measurements with varying water level. They also suggest that strong discrepancies exist between measurements conducted with the same protocols but at different locations on the dyke (crest and flank in this case).

3.3. Correction of topographic effects using computed geometric factors

The synthetic ERT data set obtained from FEM computation for the four models presented in Fig. 4 has been inverted using the analytical geometric factors K_a and the computed geometric factors K_c obtained with a water level of 0 m (no water in the canal) for confA and confC and a water level of 0.7 m below the dyke crest for confB and confD. Results are presented in Fig. 7 and are summarized in Table 2. Fig. 7a and b present the results for the pure topographic configuration confA (i.e. measurements along a homogeneous dyke without resistivity contrasts with bedrock and without water in the canal; Fig. 4a). Mean and median resistivity are equivalent with values of 60 Ω.m and 50 Ω.m for the analytic and computed geometric factor, respectively (Table 2). These results indicate that, in the case of a pure topographic effect and even with a complex topography, it is possible to retrieve a good estimate of the ground resistivity by using a more realistic geometric factor. In this case, using K_a results in an average overestimation of the resistivity of 20%. Fig. 7c and d show the inversion results in the case of a homogeneous ground with a water ($\rho = 20$ Ω.m) level in the canal located 0.3 m below the dyke crest. Images indicate that, in both cases, discrepancies are present along the profile and at depth. Mean and median resistivity are very close and are of around 55 Ω.m and 50 Ω.m for K_a and K_c, respectively. Once again, these results suggest that taking into account surface effects allows retrieving more realistic resistivity ground values. However, Fig. 7d shows a more heterogeneous distribution of resistivity and suggests that topographic correction only is not sufficient to account for the lateral presence of water. The lower resistivity values obtained with K_a in this case (confB in Fig. 4b) relative to confA (Fig. 4a) suggest that the presence of low resistivity water in the canal with respect to ground resistivity tends to counterbalance the increase in resistivity caused by using K_a.

Fig. 7e and f show the resistivity sections obtained for confC (dyke over a 400 Ω.m-bedrock located at a depth of 6 m and without water in the canal). Results first show that in both cases the depth to the

Table 4
Inversion parameters and results of the experimental time-lapse dataset. RRMS: relative root mean square error. RSD: relative standard deviation.

Measurement	Date	K	Iterations	Chi^2	RRMS (%)	Model resistivity (ohm.m)		Result in Figure
						Min	Max	
1	2010/11/09	Analytical	3	1.4	4.89	26	220	X
		Corrected	3	1.03	3.2	23	211	X
2	2010/11/12	Analytical	1	1.01	0.56	25	238	10a
		Corrected	1	0.999	0.83	24	212	10b
3	2010/12/08	Analytical	2	0.9	0.97	25	241	10c
		Corrected	1	0.96	1.12	24	212	10d
4	2012/12/13	Analytical	3	0.4	0.85	27	223	10e
		Corrected	2	2	0.9	19	228	10f

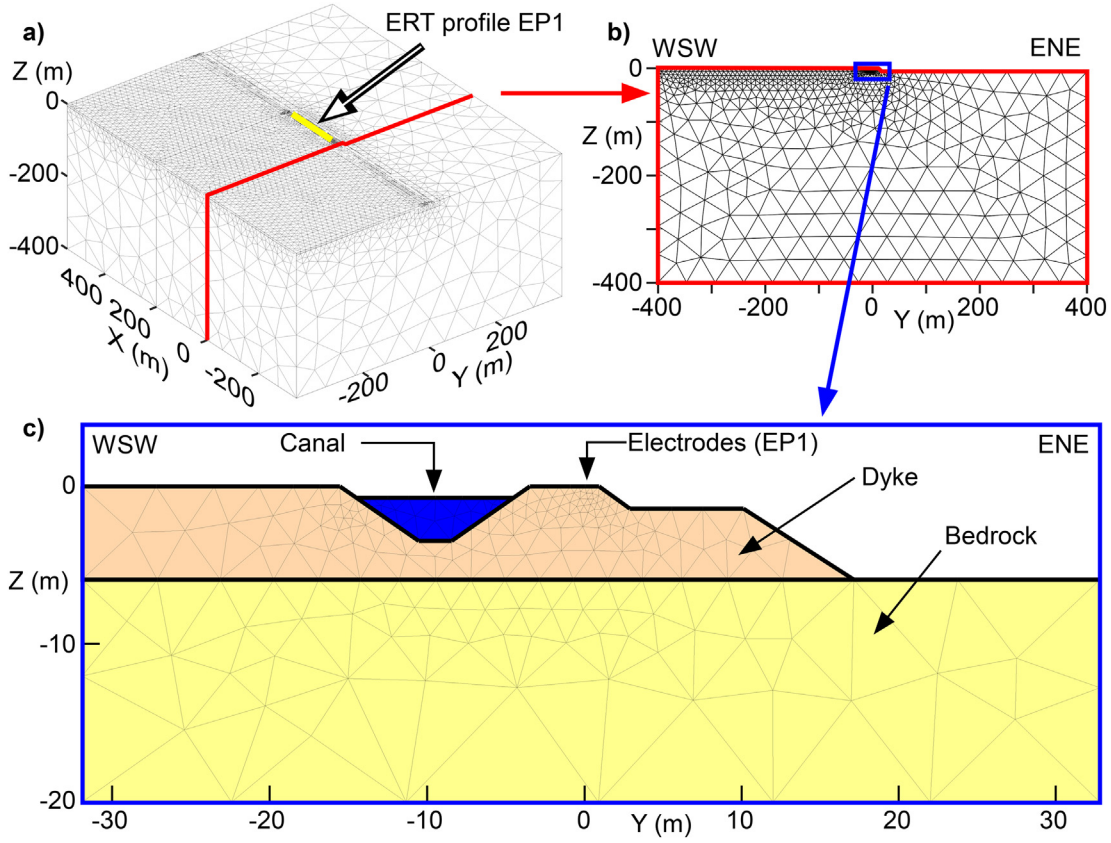

Fig. 3. Computation domain: a) General view, b) Transverse section, c) Zoom on the dyke and canal.

bedrock is identically positioned at 6 m depth. The median resistivity of the dyke appears more accurately retrieved using K_c (51.3 Ω.m) than K_a (58.7 Ω.m) as shown in Table 2. Then, the resistivity of the bedrock appears to be higher in both cases with values of up to >1500 Ω.m. However, the median resistivity of the bedrock remains in reasonable agreement with K_a (497 Ω.m) and K_c (467 Ω.m) corresponding to an overestimation of 25% and 15%; respectively.

The last model confD included both the heterogeneous resistivity distribution and a water level in the canal of 0.3 m below the dyke crest. The results are exposed in Fig. 7g and h and in Table 2. As previously observed, the interface between the dyke and the bedrock is well located at a depth of 6 m in both cases. The median resistivity of the dyke appears once again more adequate using K_c (50.8 Ω.m) than K_a (58 Ω.m) as shown in Table 2. The bedrock resistivity in this configuration is smaller than the resistivity of the model (median resistivity of 369 Ω.m and 324 Ω.m with K_a and K_c, respectively, corresponding to an underestimation of 8% and 19%, respectively). However, the mean resistivity is very close to the imposed value using K_c with an overestimation lower than 3%. These results suggest that for large AB spacings which investigate the bedrock, the water in the canal strongly influences the measurements (Cf Fig. 5). The topographic correction alone is not able to fully account for the 3D resistivity distribution within the subsurface.

To summarize, these numerical results indicate that it is possible to retrieve more realistic resistivity values by computing 3D topography effects which influence 2D inversion results. The proposed methodology consists of computing an a priori correction of geometric factors based on simple topographic measurements. It is particularly well adapted in the context of dyke survey since these data can be easily acquired in the field. However, it must be stressed out that these topographic corrections do not allow to fully correct the measured resistivity from 3D effects (such as 3D resistivity distribution). Measurements are

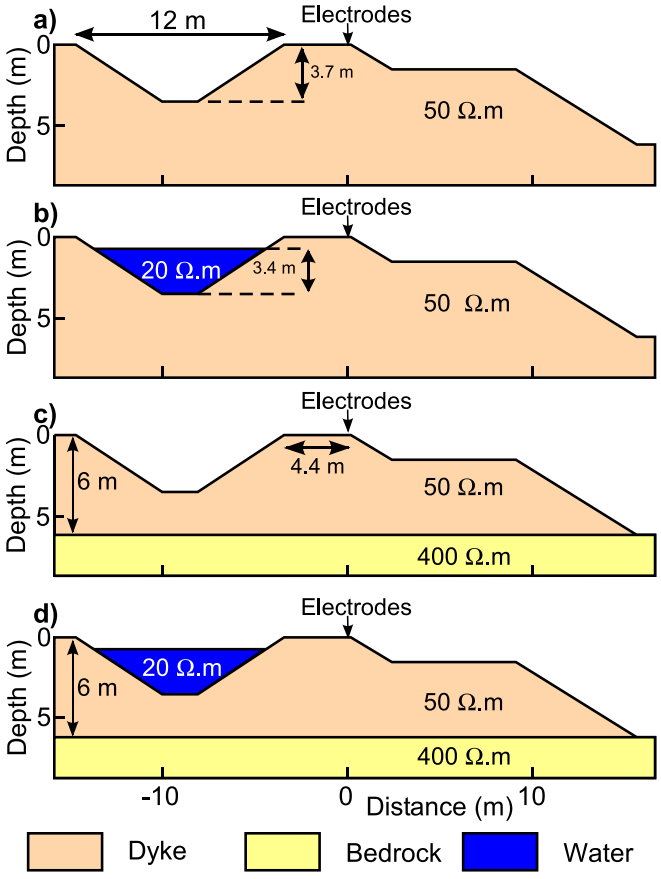

Fig. 4. Geometry and electrical properties of the synthetic models. a) to d) Configurations confA to confD, respectively.

still conducted in 2D in a strongly 3D context. As such, the 2D assumption is not valid and the retrieved resistivities cannot be considered as true ones.

4. Results on experimental data

4.1. Electrical resistivity profiles

Prior to installing the permanent monitoring system, repeatability measurements were conducted along a profile of 64 electrodes 1 m apart (from 0 m to 63 m along EP1 in Fig. 1). It corresponds to measurement 0 in Fig. 2 and in Table 1. 1305 measurements in a Wenner-Schlumberger configuration were repeated twice during a day. The maximum electrical resistivity difference between the measurements is 1.67%, with a median of 0.05%. These results indicate that the site presents low noise and that it is possible to perform time-lapse measurements which might potentially show small electrical differences.

Fig. 8a and b present the reference section of profile EP1 (measurement 1 in Fig. 2 and Table 1) inverted with the analytic geometric factor K_a (Fig. 8a) and with the computed one K_c obtained with the filled canal topography (Fig. 8b), respectively. In the same way, Fig. 8c and d expose the results for profile EP2.

Fig. 8a and c present the reference section of profile EP1 (measurement 1 in Fig. 2 and Table 1) and of profile EP2 inverted with the analytic geometric factor K_a. Inversions provided good quality results for both profiles (see Table 4 for details about EP1) with chi^2 around 1 and RRMS errors below 5%. The resistivity distribution inverted with K_a on EP1 (Fig. 8a) and on EP2 (Fig. 8c) exhibit a significant discrepancy. In order to quantify these differences, statistics on the resistivity of these sections were computed for the dyke and the bedrock (Table 3). 2 zones between 20 m and 107 m along the profile were selected to compute values: between 0 m and 2 m depth for the dyke and between 4 m and 7 m for the bedrock. In the dyke, the average value of resistivity for EP1 is higher than the one for EP2 with a relative difference of 31% between the two profiles (29% on the median value). A similar trend is observed at depth in the bedrock with a relative difference of 31.5% on the average value (42% on the median value). Given the vicinity of the two profiles, it seems very unlikely that these differences could be caused by a varying geotechnical context. Using the methodology proposed in this work, geometric factors K_c were computed for EP1 and EP2 with respect to its electrode locations for a topography corresponding to the filled canal. Results using K_c for EP1 and EP2 are presented in Fig. 8b and d, respectively. As observed with numerical modelling (see section 3), both images using K_a and K_c exhibit the same geometry but show resistivity differences. Images show a global decrease of resistivity for EP1 and an increase for EP2. The average relative difference for the dyke zone decreases down to 2.2% using K_c (Table 3). The correction of geometric factors thus provides a significant improvement of the agreement between the two profiles. However, for the bedrock, the inversion with K_c drives a decrease of resistivity for both EP1 and EP2 of about 10% keeping the relative difference between the two profiles globally unchanged. This suggests that using computed geometric factors is efficient to retrieve more realistic resistivity at the surface while, at depth, the 3D distribution of resistivity may predominantly influence the data.

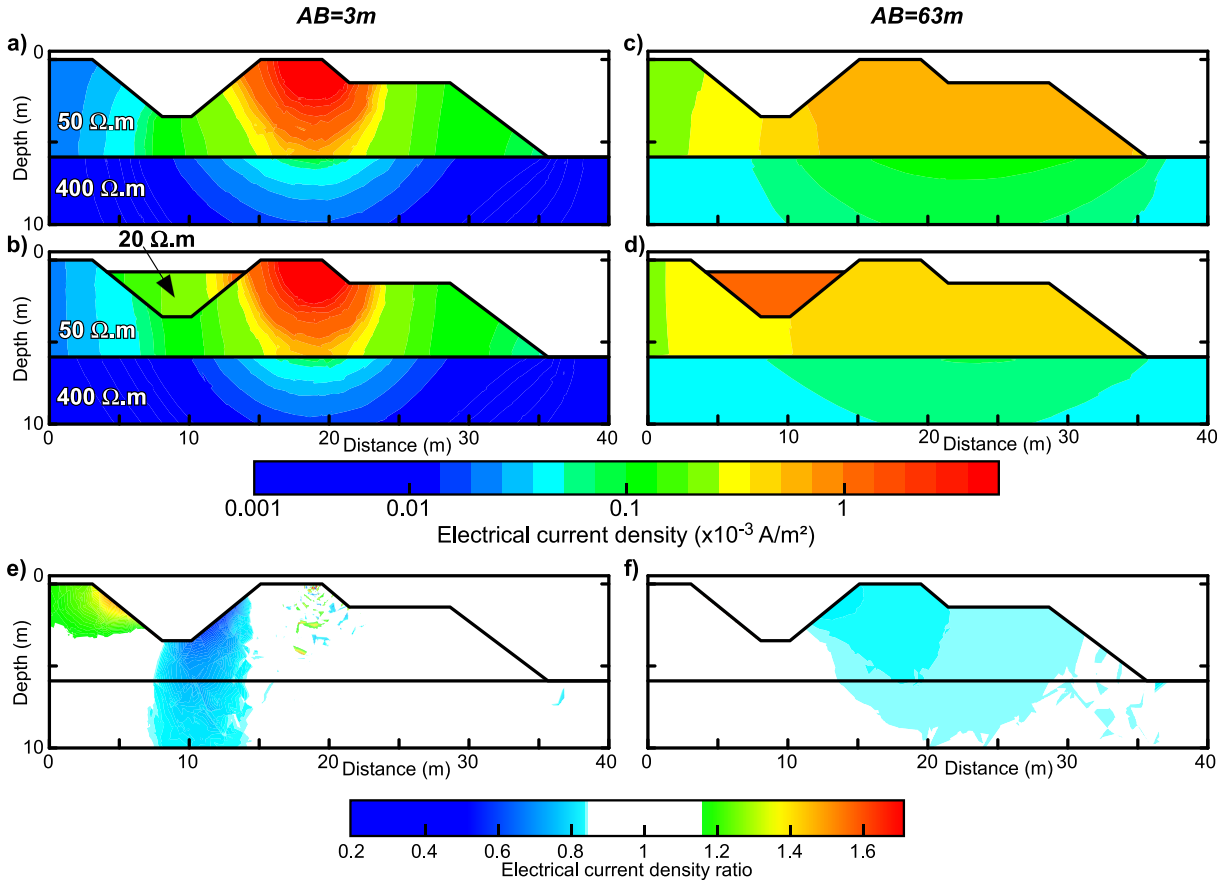

Fig. 5. Electrical current density distribution within the ground for two current electrode spacing AB of 3 m (a and b) and 63 m (c and d) and for two water heights into the canal: 0 m (a and c) and 3.4 m (b and d). The simulated transmitted current is 0.1 A. e) and f) present the electrical current density ratio between the canal filled with water and the empty canal, for a current electrode spacing AB of 3 m and 63 m, respectively. The white colour represents ratios between 0.85 and 1.15.

4.2. Comparison with EM31 measurement on EP1

The mean resistivity (using K_a and K_c) extracted from the first 2 m below ground along EP1 is presented in Fig. 9 along with the apparent resistivity measured with an EM31 device with vertical coplanar loops. Both profiles show a general and slight decrease of resistivity at both ends of the profile (between 50 Ω.m and 100 Ω.m) relative to the centre of the profile (30 Ω.m to 40 Ω.m). All three profiles show a relative trend in agreement except for two specific zones between 40 m and 60 and from 110 m to the end of the profile. However, the discrepancy observed between ERT and EM31 at the end of the profile reveals a comparable evolution of the resistivity but with different amplitudes. This suggests that these anomalies are caused at depth, where the sensitivity of EM31 is much lower than the sensitivity of ERT. Results indicate lower resistivity with K_c relative to K_a (range between 4% and 30% with a mean of 14.2%) as suggested by the numerical study (section 3). The absolute value of resistivity obtained with K_c (minimum, maximum and mean of 32 Ω.m, 82 Ω.m, and 49 Ω.m, respectively) is in much better agreement with the apparent resistivity measured with the EM31 (minimum, maximum and mean of 39 Ω.m, 55 Ω.m, and 45 Ω.m, respectively) when compared to the resistivity obtained using K_a (minimum, maximum and mean of 37 Ω.m, 97 Ω.m, and 57 Ω.m, respectively).

4.3. Monitoring results

The results of time-lapse measurements are presented in Fig. 10 as resistivity ratio between the considered measurement and measurement 1 taken as reference. Inversion parameters and results are exposed in Table 4. From a general point of view, all inversions with K_a and K_c provided satisfactorily numerical results with chi^2 values around 1 and RRMS errors below 5% (Table 4).

Measurements 1 (reference) and 2 were conducted three days apart. The main difference is the decrease of the water level in the canal (−1.65 m). The induced decrease of the water table in the dyke is comparatively small (−0.35 m; Fig. 2 and Table 1). Both sections present small resistivity changes. However, the inversion with K_a (Fig. 10a) exhibits a small increase in resistivity in the bedrock between the two measurements. On the contrary, the inversion with K_c (Fig. 10b) exhibits resistivity ratios around 1 for both the dyke and the bedrock. Considering the small variation of the water table level between the two measurements, it is not realistic that a desaturation occurred at depth in the bedrock. This suggests that a slight change in surface morphology (1.65 m for the water in the canal) is sufficient to induce artificial resistivity variations while using K_a. On the contrary, K_c allows retrieving identical resistivity between the two measurements.

Fig. 10c and d show time-lapse resistivity sections 3 measured 29 days after the reference measurement. They exhibit identical trends for the dyke: higher resistivity in the top first m and no change in the bottom part of the dyke. The increase in resistivity in the near surface, 29 days after reference measurement, is most probably related to a decrease in water content following the drop of the water table in the dyke (Fig. 2 and Table 1). The lower part of the dyke remains in the same electric, and hence hydrologic, conditions. The bedrock presents increases of resistivity up to 10% for the K_a inversion (Fig. 10c) whereas it does not change for the K_c inversion (Fig. 10d). In Fig. 10c, several resistivity decrease locations are visible at 22 m, 28 m and 38 m along the profile. They are located at the interface between the dyke and the bedrock, and at a depth of around 3.4 m. In

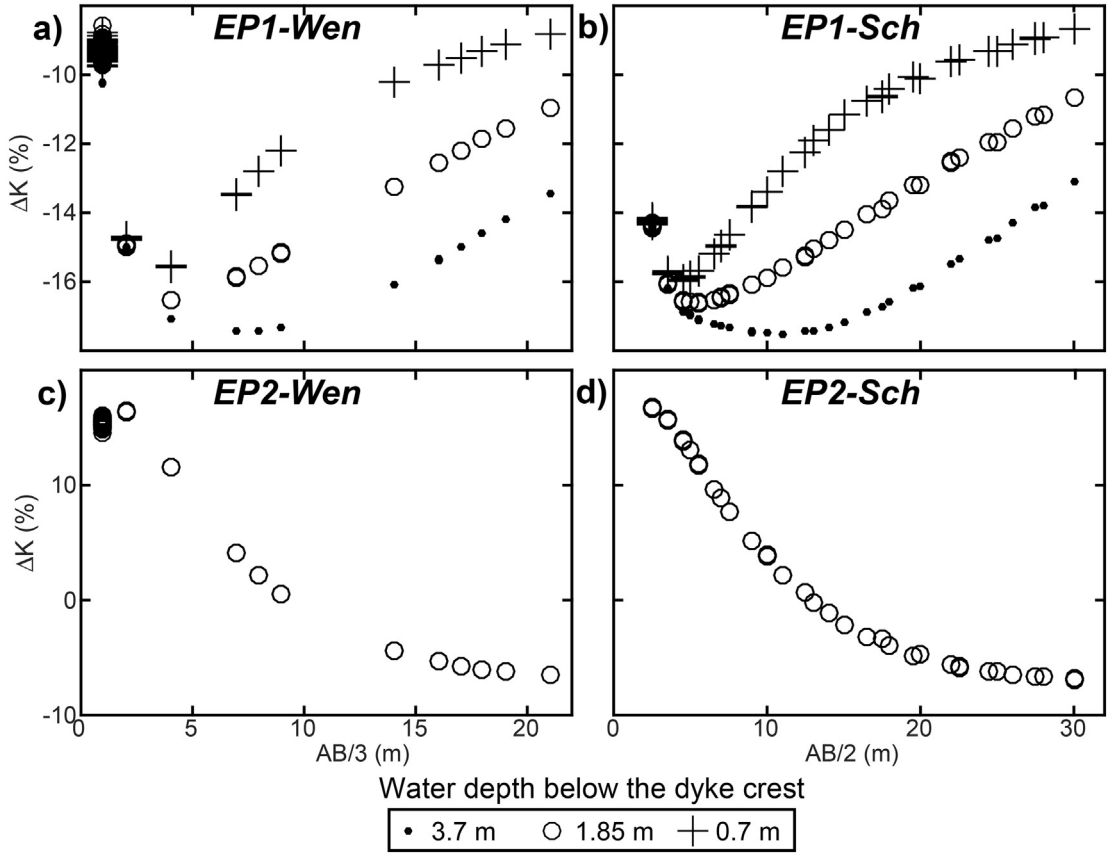

Fig. 6. Geometric factor variation induced by the geometric correction relative to the analytical formula as a function of the pseudo-depth and for varying water levels in the canal (3.7 m, 1.85 m and 0.7 m below the dyke crest). Profile EP1 in a) Wenner configuration and in b) Schlumberger configuration. Profile EP2 in c) Wenner configuration and in d) Schlumberger configuration.

Fig. 10d, the resistivity decrease at a distance of 38 m, corresponding to the repaired leaking zone (LZ1), appears much more distinctly. However, the conductive anomaly appears to propagate at depth. Remediation works consisted of injecting clays within the leakage zone. As a consequence wet clays, with a resistivity lower than the resistivity of the dyke and of the water, induced a decrease in resistivity (and thus a resistivity ratio lower than 1 on the time-lapse sections). Both sections (with K_a and K_c) detected LZ1. As observed in the synthetic data (section 3.2), the computed geometric factors appear to provide a small correction on the structural delineation (of the bedrock interface and LZ1). It essentially leads to a general but non-uniform decrease of the inverted resistivities compared to those obtained with the analytic geometric factors. Nevertheless, the estimation of the absolute value of resistivities is probably more realistic.

Fig. 10e and f present the time-lapse resistivity sections 34 days after reference measurement 1. The water table in the canal and in the dyke was located 0.7 m and 0.6 m below the dyke crest, respectively (i.e. 1.25 m and 0.3 m higher than for reference measurement 1, respectively; Fig. 2 and Table 1). The first 2 m below the ground present higher ratios than previously, probably related to an ongoing decrease in water content. The lower part of the dyke does not exhibit resistivity variations, suggesting that despite the difference in saturation, the difference in water content was not sufficient enough to generate resistivity variations. The bedrock resistivity is constant in the case of the uncorrected measures (Fig. 10e) and shows a slight increase in resistivity (up to 15%) in the case of the corrected resistivity (Fig. 10f). This might very probably be linked to an ongoing decrease in water content in the bedrock despite the increase of the water table in the canal and in the dyke. The uncorrected resistivity ratio section still shows the three same locations of the decrease in resistivity at 22 m, 28 m and 38 m along the profile with a decrease of up to 25% for LZ1. Using K_c the main negative anomaly in the image corresponds to LZ1 only. It can also be noticed that LZ2 was never identified on the images, probably because of a too small size.

5. Discussion and conclusion

A static and time-lapse ERT survey has been performed during repair works on a small canal earth-filled dyke in the centre of France. This study provided the opportunity to explore the effect of 3D topographic effects on the inversion of 2D ERT sections measured along the crest of the dyke or on its mid-slope. Synthetic datasets were computed by direct numerical simulation of the direct current problem corresponding to the ERT acquisition. Considering the effect of the topography only (constant electrical resistivity), the computed geometrical factors (K_c) exhibited differences with the classical analytical set of geometric factors for a flat infinite half space configuration (K_a) resulting in values between −8% and − 18% for sections measured along the crest of the dyke and between +18% and − 8% for sections measured along its mid-slope. Unlike the results reported by Sjödahl et al. (2006), the evolution of apparent resistivity (caused by a distortion of the geometric factor compared to the analytic formula) as a function of electrode spacing exhibits a maximum underestimation at intermediate depth for sections measured along the crest of the dyke (between 4 m and 12 m depending on the electrode configuration and the topography). However, they studied a large trapezoid-shaped dam with a simpler topography than the geotechnical structure studied here. While using a 2.5D modelling approach, Sjödahl et al. (2006) managed to detect

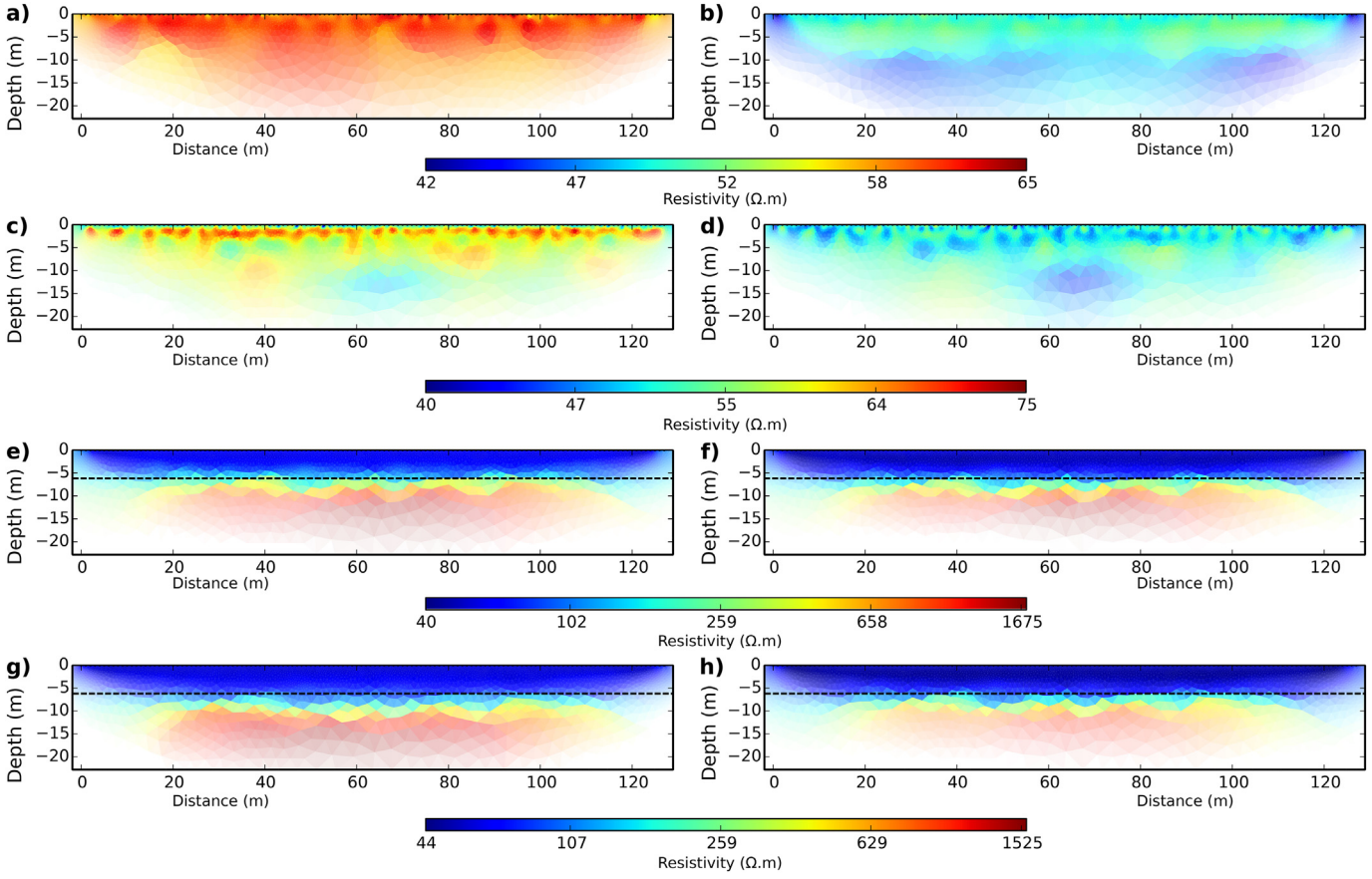

Fig. 7. synthetic results. a), c), e), g): 2D inversion results using the analytical geometric factor. b), d), f), h): 2D inversion results using a geometric factor corrected from topography. See Table 2 for quantitative details.

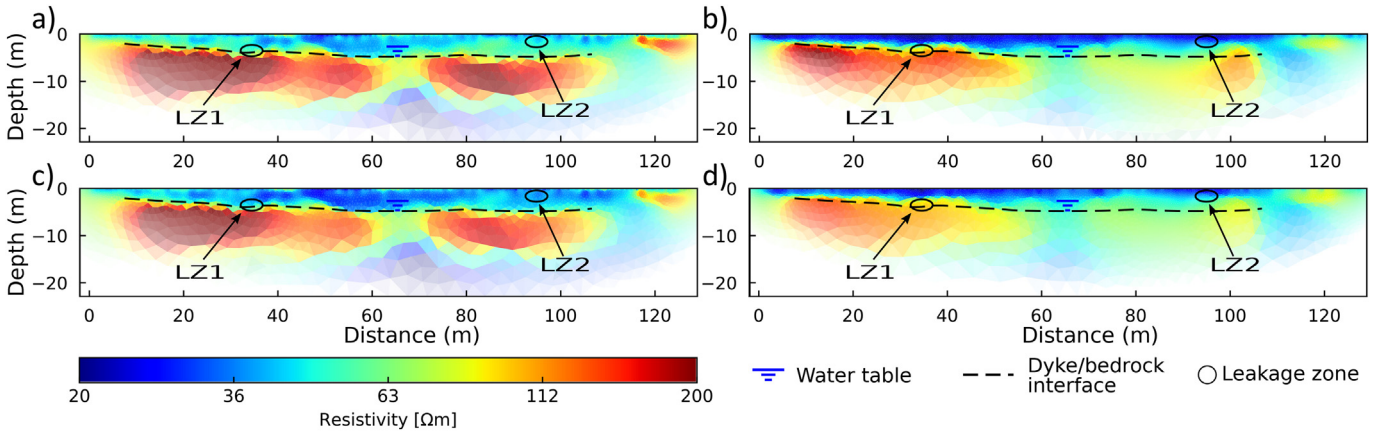

Fig. 8. Resistivity sections of profiles EP1 (reference measurement number 1 in Fig. 2) a) using K_a and b) using K_c and of profile EP2 **c)** using K_a and d) using K_c. The black circles correspond to the localization of two observed leakage zones LZ1 and LZ2 (Bièvre et al., 2017).

flat and elongated damage zones. The results presented here show that it is possible to better detect small and circular-shaped damage zones using a full 3D modelling approach which is in agreement with comments by Sjödahl et al. (2006).

Using these computed geometrical factors in the inversion of various synthetic ERT datasets improved the agreement between the inverted resistivity section and the original model for all the tested dyke models. These tests included homogeneous and heterogeneous electrical resistivity distributions. The improvement was observed in both absolute values of electrical resistivities and locations of heterogeneities. Results also showed that in both cases (using K_a and K_c) the depth to interfaces between the dyke and the bedrock does not change and that the applied correction only tends to correct resistivity values. Also, it appears that for large electrode spacings and with a 3D underground resistivity distribution, the full knowledge of the underground resistivity (water and ground) would be needed to retrieve adequate values. These observations are in agreement with findings by Fargier et al. (2014). Our results finally suggest that, when conducting resistivity measurements with profiles along the dyke stretch, it is possible to correct for topographical effects only. Possible further bias might originate from the 3D underground resistivity distribution (i.e. the electrical properties of the ground are not constant in the direction perpendicular to the electrode spread). These effects cannot be taken into account by a 2D approach. Contrarily to Fargier et al. (2014) who proposed to introduce a priori information regarding the 3D underground distribution of resistivity, it is here assumed that this approach may lead to bias and possible artefacts in case of local and non-identified resistivity variation. It is here proposed to introduce only known, and easy to measure information. Cho et al. (2014) recently proposed to use a combined model (made of a combination of models, namely the reference time section and the time-lapse sections, inverted separately) to get rid of the effects of changing water level in the reservoir. However, this approach failed to detect leakage zones when water level changes were large. The method proposed here shows that it is feasible to retrieve realistic resistivity distribution by using a simple approach which consists in computing the geometric factor each time the water level changes.

The resistivity deduced from ERT in the top 3 m of the dyke body was integrated and compared with EM31 measurements. Results obtained with K_c provided a fair agreement with EM31 measurements. The resistivity inverted with K_c presented a mean shift of approximately −14% in the zone of interest located between the dyke and the bedrock when compared with sections inverted with K_a. These experimental results (comparison of K_a and K_c results) and the observed resistivity shift are in agreement with the results of the numerical study. These results were also confirmed by the comparison of resistivity values between two adjacent profiles (EP1 and EP2) exhibiting resistivity discrepancies although being located in the same geotechnical context. The computation of topography-corrected geometric factors and resistivity allowed to retrieve identical resistivity for the dyke. At depth, however, the resistivity difference for the bedrock remained the same. It is here suggested that at depth the 3D underground resistivity distribution has a predominant influence on the measurements compared to the topographic effect.

The proposed methodology allows improving the analysis of dyke structure using ERT measurement. The four main steps of the approach

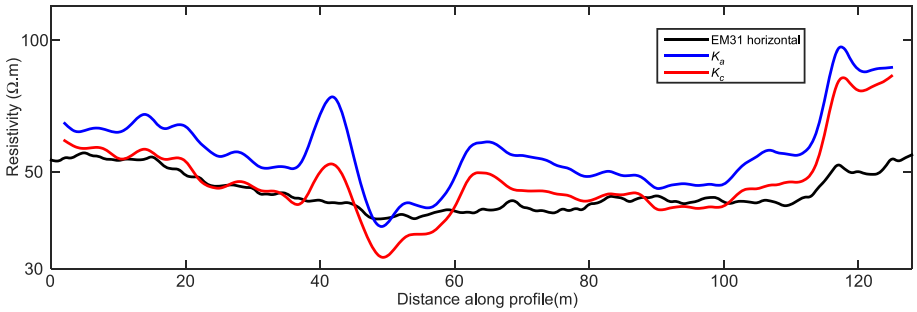

Fig. 9. Comparison between the resistivity of the first 3 m below ground along profile EP1 with different techniques: EM31 (vertical coplanar loops) and mean resistivity extracted from ERT measurement 1 in Fig. 2. Resistivity from ERT is shown for both analytical (*Ka*) and topography-corrected (*Kc*) values.

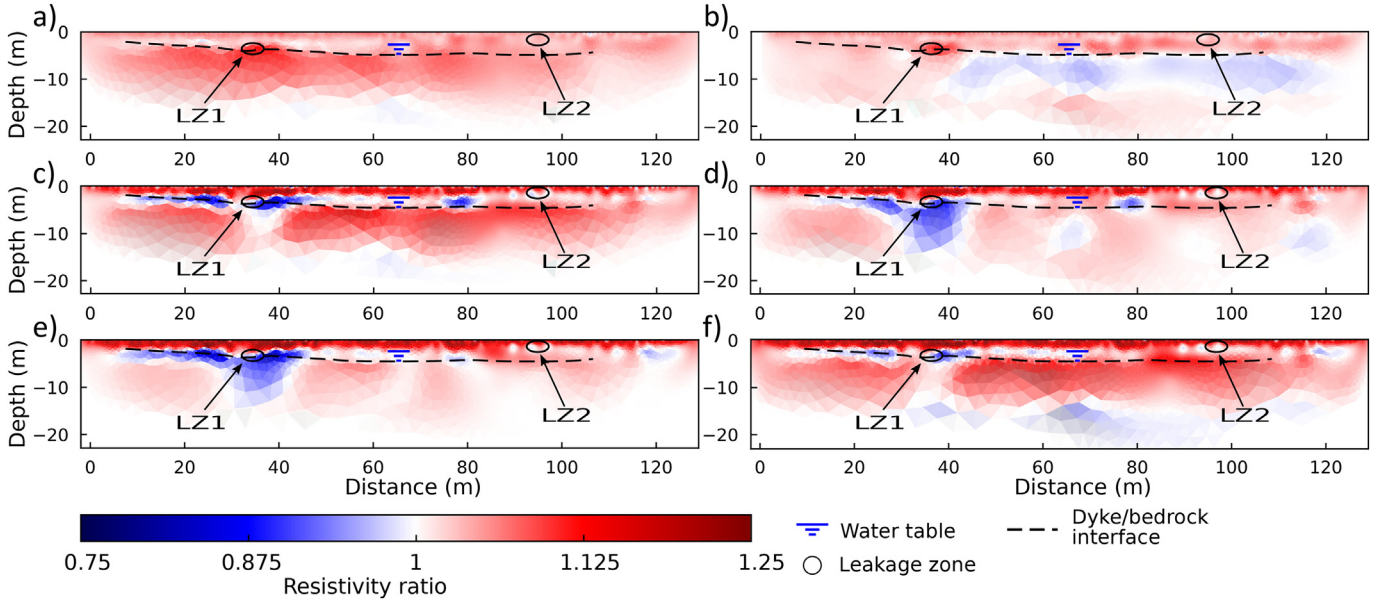

Fig. 10. Time-lapse inversion results. The black circles correspond to the localization of leakage zones (Bièvre et al., 2017) and the dashed line to the interface between the dyke and the bedrock. a), c) and e) Resistivity variations with the analytical geometric factor K_a. b), d) and f) Resistivity variations with the geometric factor corrected from the topographic effect K_c. LZ1 and LZ2: leakage zones 1 and 2.

can be described as **1)** ERT measurements along the structure using a classic methodology, **2)** topography measurement, **3)** numerical estimation of the geometric factor induced by the surface morphology and the water level and, finally, **4)** inversion of the apparent resistivity (static or time-lapse) recalculated using the geometric factor deduced in step 3. Based on a simple correction of geometric factors deduced from numerical computation, it could be easily applied to a practical situation since it only requires measuring the surface topography of the study site. Such an approach may also improve the quality of 2D ERT surveys performed on sites presenting a complex and strong 3D topography such as, among others, landslides, engineered slopes and mountainous areas.

Acknowledgements

This work was supported by the French IFSTTAR-CEREMA DOFEAS Program. Rémi Clément (IRSTEA) is acknowledged for providing the F3DM package and for numerous discussions on ERT numerical modelling. Grégory Bièvre and Laurent Oxarango are part of LabEx OSUG@2020 (ANR10 LABX56). The authors thank the anonymous reviewers for their comments which helped to improve the manuscript.

References

Bièvre, G., Jongmans, D., Winiarski, T., Zumbo, V., 2012. Application of geophysical measurements for assessing the role of fissures in water infiltration within a clay landslide (Trièves area; French Alps). Hydrol. Process. 26:2128–2142. https://doi.org/10.1002/hyp.7986.

Bièvre, G., Lacroix, P., Oxarango, L., Goutaland, D., Monnot, G., Fargier, Y., 2017. Integration of geotechnical and geophysical techniques for the characterization of a small earth-filled canal dyke and the localization of water leakage. J. Appl. Geophys. 139:1–15. https://doi.org/10.1016/j.jappgeo.2017.02.002.

Cardarelli, E., Cercato, M., Filippo, G., 2010. Geophysical investigation for the rehabilitation of a flood control embankment. Near Surf. Geophys. 8:287–296. https://doi.org/10.3997/1873-0604.2010018.

Cardarelli, E., Cercato, M., De Donno, G., 2014. Characterization of an earth-filled dam through the combined use of electrical resistivity tomography; P- and SH-wave seismic tomography and surface wave data. J. Appl. Geophys. 106:87–95. https://doi.org/10.1016/j.jappgeo.2014.04.007.

Cho, I.-K., Yeom, J.-Y., 2007. Crossline resistivity tomography for the delineation of anomalous seepage pathways in an embankment dam. Geophysics 72:G31–G38. https://doi.org/10.1190/1.2435200.

Cho, I.-K., Ha, I.-S., Kim, K.-S., Ahn, H.-Y., Lee, S., Kang, H.-J., 2014. 3D effects on 2D resistivity monitoring in earth-fill dams. Near Surf. Geophys. 12:73–81. https://doi.org/10.3997/1873-0604.2013065.

Clément, R., Moreau, S., 2016. How should an electrical resistivity tomography laboratory test cell be designed? Numerical investigation of error on electrical resistivity measurement. J. Appl. Geophys. 127:45–55. https://doi.org/10.1016/j.jappgeo.2016.02.008.

Fargier, Y., Palma Lopes, S., Fauchard, C., Francois, D., Côte, P., 2014. DC-electrical resistivity imaging for embankment dike investigation: a 3D extended normalisation approach. J. Appl. Geophys. 103:245–256. https://doi.org/10.1016/j.jappgeo.2014.02.007.

Fox, R.C., Hohmann, G.W., Killpack, T.J., Rijo, L., 1980. Topographic effects in resistivity and induced-polarization surveys. Geophysics 45:75–93. https://doi.org/10.1190/1.1441041.

Günther, T., Rücker, C., Spitzer, K., 2006. Three-dimensional modelling and inversion of DC resistivity data incorporating topography - II. Inversion. Geophys. J. Int. 166:506–517. https://doi.org/10.1111/j.1365-246X.2006.03011.x.

Hayley, K., Bentley, L.R., Gharibi, M., Nightingale, M., 2007. Low temperature dependence of electrical resistivity: implications for near surface geophysical monitoring. Geophys. Res. Lett. 34, L18402. https://doi.org/10.1029/2007GL031124.

Hayley, K., Bentley, L.R., Pidlisecky, A., 2010. Compensating for temperature variations in time-lapse electrical resistivity difference imaging. Geophysics 75:WA51–WA59. https://doi.org/10.1190/1.3478208.

Hennig, T., Weller, A., Canh, T., 2005. The effect of dike geometry on different resistivity configurations. J. Appl. Geophys. 57 (4):278–292. https://doi.org/10.1016/j.jappgeo.2005.03.001.

LaBrecque, D.J., Yang, X., 2001. Difference inversion of ERT data: a fast inversion method for 3-D in situ monitoring. J. Environ. Eng. Geophys. 6:83–89. https://doi.org/10.4133/JEEG6.2.83.

McNeill, J.D., 1980. Electrical Terrain Conductivity Measurement at Low Induction Numbers. Geonics Ltd, Mississauga, Canada Available at:. www.geonics.com.

Minsley, B.J., Burton, B.L., Ikard, S., Powers, M.H., 2011. Hydrogeophysical investigations at hidden dam, Raymond, California. J. Environ. Eng. Geophys. 16 (4):145–164. https://doi.org/10.2113/JEEG16.4.145.

Niederleithinger, E., Weller, A., Lewis, R., 2012. Evaluation of geophysical techniques for dike inspection. J. Environ. Eng. Geophys. 17 (4):185–195. https://doi.org/10.2113/JEEG17.4.185.

Rücker, C., Günther, T., Spitzer, K., 2006. Three-dimensional modelling and inversion of DC resistivity data incorporating topography - I. Modelling. Geophys. J. Int. 166:495–505. https://doi.org/10.1111/j.1365-246X.2006.03010.x.

Samouëlian, A., Cousin, I., Tabbagh, A., Bruand, A., Richard, G., 2005. Electrical resistivity survey in soil science: a review. Soil Tillage Res. 83:173–193. https://doi.org/10.1016/j.still.2004.10.004.

Sjödahl, P., Dahlin, T., Zhou, B., 2006. 2.5D resistivity modeling of embankment dams to assess influence from geometry and material properties. Geophysics 71:G107–G114. https://doi.org/10.1190/1.2198217.

Sjödahl, P., Dahlin, T., Johansson, S., Loke, M., 2008. Resistivity monitoring for leakage and internal erosion detection at Hallby embankment dam. J. Appl. Geophys. 65:155–164. https://doi.org/10.1016/j.jappgeo.2008.07.003.

Sjödahl, P., Dahlin, T., Johansson, S., 2009. Embankment dam seepage evaluation from resistivity monitoring data. Near Surf. Geophys. 7:463–474. https://doi.org/10.3997/1873-0604.2009023.

Telford, W.M., Geldart, L.P., Sheriff, R.E., 1990. Applied Geophysics. 2nd. Cambridge University Press, Cambridge; UK.

Waxman, M.H., Thomas, E.C., 1974. Electrical conductivities in shaly sands: I. The relation between hydrocarbon saturation and resistivity index; II. The temperature coefficient of electrical conductivity. J. Pet. Technol. 26, 213–225.

Weller, A., Canh, T., Breede, K., Vu, N.T., 2006. Multi-electrode measurements at Thai Binh dikes (Vietnam). Near Surf. Geophys. 4:135–143. https://doi.org/10.3997/1873-0604.2005039.

Weller, A., Lewis, R., Canh, T., Möller, M., Scholz, B., 2014. Geotechnical and geophysical long-term monitoring at a levee of Red River in Vietnam. J. Environ. Eng. Geophys. 19:183–192. https://doi.org/10.2113/JEEG19.3.183.